

C5-Functionalized DNA, LNA, and α -L-LNA: Positional Control of Polarity-Sensitive Fluorophores Leads to Improved SNP-Typing**

Michael E. Østergaard,^[a] Pawan Kumar,^[a, b] Bharat Baral,^[a] Dale C. Guenther,^[a] Brooke A. Anderson,^[a] F. Marty Ytreberg,^[c] Lee Deobald,^[d] Andrzej J. Paszczyński,^[d] Pawan K. Sharma,^[b] and Patrick J. Hrdlicka*^[a]

Abstract: Single nucleotide polymorphisms (SNPs) are important markers in disease genetics and pharmacogenomic studies. Oligodeoxyribonucleotides (ONs) modified with 5-[3-(1-pyrenecarboxamido)propynyl]-2'-deoxyuridine monomer **X** enable detection of SNPs at non-stringent conditions due to differential fluorescence emission of matched versus mismatched nucleic acid duplexes. Herein, the thermal denaturation and optical spectroscopic characteristics of monomer **X** are compared to the corresponding locked nucleic acid (LNA) and α -L-LNA monomers **Y** and **Z**. ONs modified with

monomers **Y** or **Z** result in a) larger increases in fluorescence intensity upon hybridization to complementary DNA, b) formation of more brightly fluorescent duplexes due to markedly larger fluorescence emission quantum yields ($\Phi_F=0.44-0.80$) and pyrene extinction coefficients, and c) improved optical discrimination of SNPs in DNA targets. Optical spectroscopy studies suggest that the nucleobase moieties of mono-

mers **X-Z** adopt *anti* and *syn* conformations upon hybridization with matched and mismatched targets, respectively. The polarity-sensitive 1-pyrenecarboxamido fluorophore is, thereby, either positioned in the polar major groove or in the hydrophobic duplex core close to quenching nucleobases. Calculations suggest that the bicyclic skeletons of LNA and α -L-LNA monomers **Y** and **Z** influence the glycosidic torsional angle profile leading to altered positional control and photophysical properties of the C5-fluorophore.

Keywords: bicyclic nucleotides • BNA • DNA targeting • pyrene • single nucleotide polymorphisms

Introduction

Single nucleotide polymorphisms (SNPs) are the most frequently occurring genetic variation in the human genome (>9 million SNPs, one SNP per 1000 base pairs).^[1] SNPs often result in phenotypic changes, and are accordingly important markers in disease genetics and pharmacogenomic studies. The most established SNP genotyping technologies are enzyme-based or rely on small differences in thermosta-

bility between duplexes of probes and complementary or SNP-containing targets.^[1,2] Moreover, these multistep protocols often necessitate stringent control of assay conditions (e.g., temperature, ionic strength). As a result, there has been a major thrust to develop alternative SNP-typing approaches, which are operationally more simple and cost-efficient. Examples include modified molecular beacons,^[3] dual probes,^[4] quenched autoligation probes,^[5] intercalator-modified probes,^[6] charge transfer based approaches,^[7] and base-discriminating fluorescent (BDF) probes.^[8] Oligodeoxyribonucleotides (ONs) modified with 5-[3-(1-pyrenecarboxamido)propynyl]-2'-deoxyuridine monomer **X** (Figure 1) have emerged as particularly promising BDF probes due to their efficient optical discrimination of complementary over mismatched targets and moderately high fluorescence quantum yields,^[8d] which has enabled discrimination of SNPs in human breast cancer cell lines at 50 nM target concentration.^[9] Molecular modeling and photophysical studies suggest that the polarity-sensitive 3-(1-pyrenecarboxamido)propynyl moiety of monomer **X** (Figure 1) intercalates into the hydrophobic base stack upon hybridization with mismatched targets resulting in fluorescence quenching, while it points toward the polar major groove in duplexes with complementary DNA targets resulting in high fluorescence.^[8d] These differences in binding modes are suggested to correlate with changes in the glycosidic torsion angle (O4'-C1'-N1-C2) from *anti* to *syn* ranges.

[a] Dr. M. E. Østergaard, Dr. P. Kumar, B. Baral, D. C. Guenther, B. A. Anderson, Prof. P. J. Hrdlicka
Department of Chemistry, University of Idaho
P.O. Box 442343, Moscow, ID 83844-2343 (USA)
Fax: (+1)208-885-6173
E-mail: hrdlicka@uidaho.edu

[b] Dr. P. Kumar, Prof. P. K. Sharma
Department of Chemistry, Kurukshetra University
Kurukshetra 136119 (India)

[c] Prof. F. M. Ytreberg
Department of Physics, University of Idaho
P. O. Box 440903, Moscow, ID 83844-0903 (USA)

[d] Dr. L. Deobald, Prof. A. J. Paszczyński
Environmental Biotechnology Institute, University of Idaho
P. O. Box 441052, Moscow, ID 83844-1052 (USA)

[**] LNA = locked nucleic acid; SNP = single nucleotide polymorphism.

Supporting information for this article is available on the WWW under <http://dx.doi.org/10.1002/chem.201002109>.

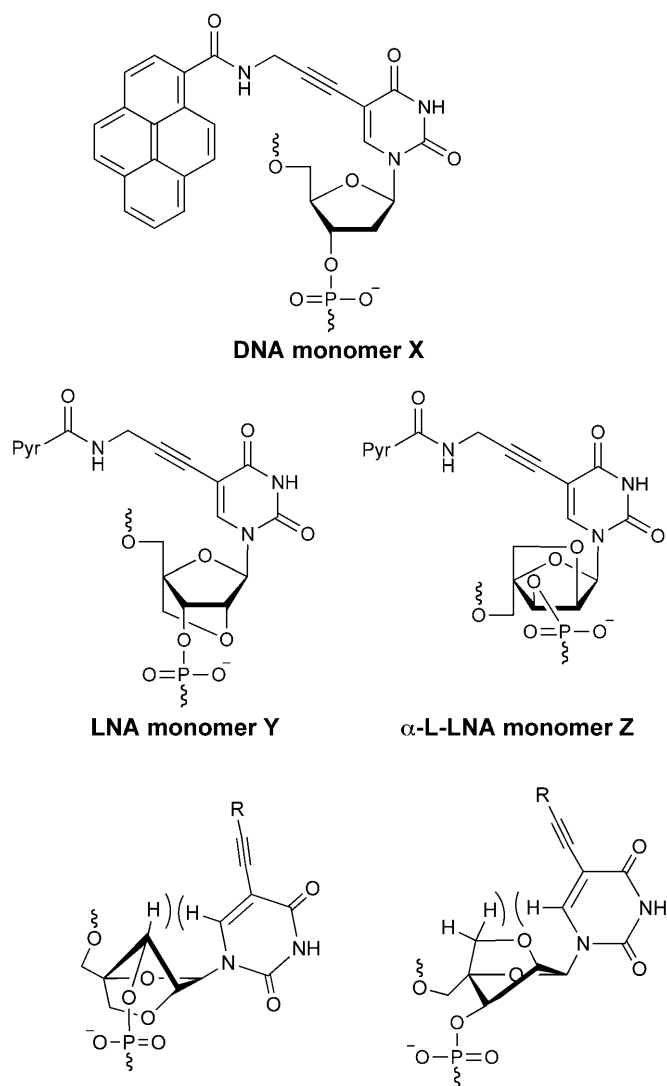


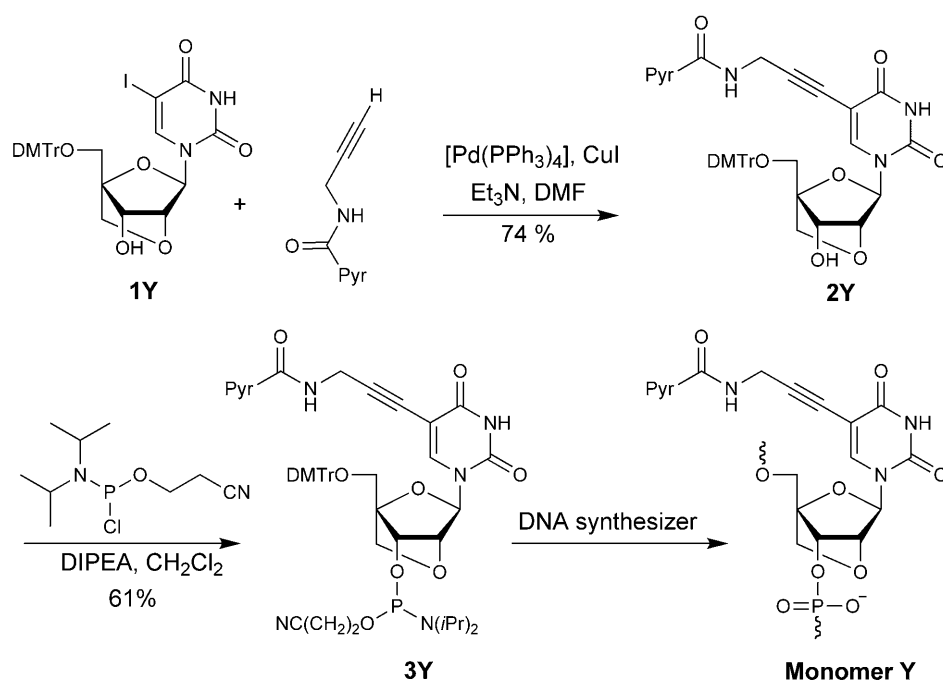
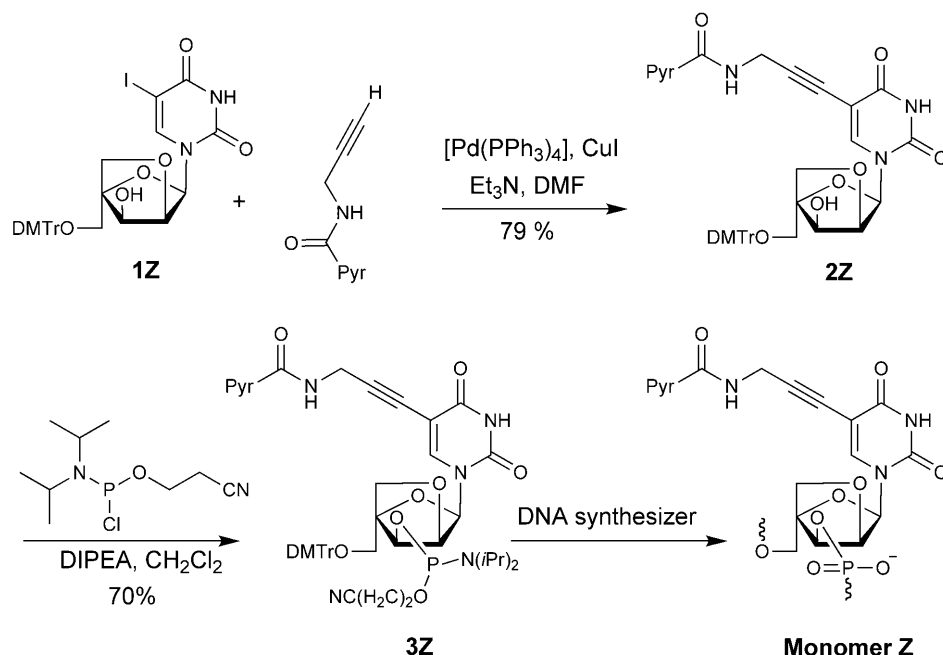
Figure 1. Chemical structures of 5-[3-(1-pyrenecarboxamido)propynyl]-2'-deoxyuridine, LNA uridine and α -L-LNA uridine monomers **X–Z** studied herein. Pyr = pyren-1-yl. Illustration of suggested interaction between H6 and furanose hydrogens.

As part of our ongoing interest in functionalized variants^[10] of LNA (Locked Nucleic Acid)^[11] and α -L-LNA,^[12] we set out to synthesize and characterize the corresponding C5-functionalized LNA and α -L-LNA monomers **Y** and **Z** in a comparative study with monomer **X** (Figure 1). We hypothesized that the extreme sugar puckering of the bicyclic LNA and α -L-LNA nucleotides^[13] would a) influence the *anti* to *syn* rotational profile due to steric hindrance between H6 and sugar protons (Figure 1), b) result in higher positional control of the polarity-sensitive 3-(1-pyrenecarboxamido)propynyl fluorophore, and c) possibly lead to improved SNP-typing properties.

Synthesis: The Sonogashira reaction between known 5-iodo-LNA uridine derivative **1Y**^[10c] and 1-pyrenylpropargylamide^[8d] afforded C5-functionalized alcohol **2Y** in 74% yield (Scheme 1). Subsequent O3'-phosphitylation using standard conditions afforded phosphoramidite **3Y** in 61% yield. The corresponding C5-functionalized α -L-LNA phosphoramidite **3Z**, that is, the first example of this class of LNAs, was obtained in an equivalent manner from **1Z** (Scheme 2; the synthesis of this intermediate will be presented elsewhere), while the 2'-deoxyuridine analogue was prepared as reported in the literature.^[8d] The identity of all new compounds was fully ascertained by NMR spectroscopy (¹H, ¹³C, ³¹P, COSY and HSQC) and HRMS, while purity was determined by 1D NMR spectroscopy (see the Supporting Information)

The phosphoramidites were used in automated solid-phase DNA synthesis (0.2 μ mol scale) to incorporate monomers **X**, **Y** and **Z** into the center of 13-mer ONs that have been previously used to study BDF probes.^[8d] The nucleotides flanking the **X/Y/Z** monomers were systematically varied to explore the influence of neighbouring nucleotides on biophysical properties (**ON5–ON16**). Coupling yields of >98% were observed during incorporation of unmodified monomers as well as for phosphoramidites **3X/3Y/3Z** using extended coupling times (15 min) and 4,5-dicyanoimidazole as an activator (see the Supporting Information) The identity and purity of the ONs was verified by MALDI-TOF MS analysis (see Table S2 in the Supporting Information) and RP-HPLC (>80%), respectively.

Thermal denaturation studies: The thermostability of duplexes between **ON5–ON16** and complementary or mismatched DNA targets was studied by UV thermal denaturation experiments using medium salt buffer conditions ([Na⁺]=110 mM) and compared to the corresponding unmodified DNA duplexes (Table 1). The UV thermal denaturation curves of all modified DNA duplexes exhibit smooth sigmoidal monophasic transitions (see Figures S1–S3 in the Supporting Information). Less pronounced hyperchromicity was observed in duplexes modified with C5-functionalized LNA monomer **Y** or α -L-LNA monomer **Z**, which indicates less efficient π – π stacking between nucleobases in the duplex.^[14] Incorporation of the known 5-[3-(1-pyrenecarboxamido)propynyl]-2'-deoxyuridine monomer **X**^[8d] into ONs (**ON5–ON8**) significantly decreases the thermal denaturation temperatures (T_m) of duplexes with DNA complements (ΔT_m between -1.5°C and -6.0°C , Table 1). Interestingly, incorporation of the corresponding C5-functionalized LNA or α -L-LNA building blocks into ONs results in similar destabilization of duplexes although with reduced sequence variability (ΔT_m between -2.0 and -4.5°C for monomer **Y**, and between -2.5 and -4.0°C for monomer **Z**, Table 1). Thus, the well-established stabilizing effects of conventional LNA^[11] and α -L-LNA^[12] monomers appear to be fully compromised by the 3-(1-pyrenecarboxamido)propynyl moiety

Scheme 1. Synthesis of monomer **Y**. DMTr = 4,4'-dimethoxytrityl.Scheme 2. Synthesis of monomer **Z**.

at the C5 position. This contrasts trends with C5-functionalized LNA carrying non-aromatic moieties, which generally are very well tolerated in nucleic acid duplexes.^[10c]

Next, the Watson–Crick specificity of **ON5–ON16** was evaluated by using DNA targets with mismatched nucleotides opposite of the site of modification. Reference strands

ON1–ON4 exhibit the expected specificity patterns, that is, a) formation of duplexes with substantially reduced thermostability, and b) less efficient discrimination of T:G mismatches compared to T:C and T:T mismatches (Table 1). Comparison with modified **ON5–ON16** in the same sequence contexts reveals that the 3-(1-pyrenecarboxamido)propynyl moiety at the C5 position markedly decreases target specificity as the following order is observed: thymidine [highest specificity] > α -L-LNA monomer **Z** > LNA monomer **Y** > DNA monomer **X** (e.g., compare mismatch ΔT_m values for **ON2**, **ON6**, **ON10**, and **ON14**, Table 1). This lends support for the hypothesis that the pyrene moiety intercalates upon hybridization with mismatched targets, as decreased mismatch specificity often is observed for monomers with intercalating units.^[10b,15] The improved mismatch discrimination of LNA monomer **Y** and α -L-LNA monomer **Z** relative to DNA monomer **X** parallels the well-established enhanced mismatch discrimination of LNA^[11a,16] and α -L-LNA,^[10b,12] although the underlying molecular mechanism leading to this effect is unknown.

Optical spectroscopy studies:

Three characteristics are of particular importance in the design of SNP probes: a) the *relative increase in fluorescence intensity upon hybridization to complementary nucleic acid targets*, since excess probe cannot be washed out in homogeneous assays, b) the *brightness of the resulting target duplexes*, defined as the product of the extinction

coefficient of the fluorophore at the applied excitation wavelength ϵ_{ex} and the fluorescence emission quantum yield Φ_{F} , since this influences detection limits, and c) the *optical discrimination of singly mismatched nucleic acid targets*, since this determines the robustness of the SNP-typing method. To fully evaluate these characteristics and gain ad-

Table 1. Thermal denaturation temperatures (T_m values) of duplexes between **ON1–ON16** and complementary (B = A) or mismatched DNA targets.^[a]

ON	Sequences	T_m (ΔT_m)	$C^{[c]}$	Mismatch ΔT_m	$T^{[c]}$
		[°C] ^[b] B = A ^[b]		[°C] ^[c] G ^[c]	
1	5'-CG CAA ATA AAC GC	48.5	-10.0	-5.0	-9.0
2	5'-CG CAA CTC AAC GC	55.5	-13.5	-7.0	-9.0
3	5'-CG CAA GTG AAC GC	55.0	-13.0	-9.5	-10.0
4	5'-CG CAA TTT AAC GC	48.5	-11.0	-9.0	-11.0
5	5'-CG CAA AXA AAC GC	45.5 (-3.5)	-4.5	-2.0	-3.0
6	5'-CG CAA CXC AAC GC	54.0 (-1.5)	-8.0	-4.0	-5.5
7	5'-CG CAA GXG AAC GC	49.0 (-6.0)	-3.5	-7.0	-4.5
8	5'-CG CAA TXT AAC GC	44.0 (-4.5)	-5.0	-4.0	-3.5
9	5'-CG CAA AYA AAC GC	45.5 (-3.0)	-5.5	-3.5	-4.5
10	5'-CG CAA CYC AAC GC	53.5 (-2.0)	-9.0	-4.5	-7.0
11	5'-CG CAA GYG AAC GC	51.5 (-3.5)	-3.5	-11.5	-6.5
12	5'-CG CAA TYT AAC GC	44.0 (-4.5)	-7.5	-6.5	-6.0
13	5'-CG CAA AZA AAC GC	44.5 (-4.0)	-7.5	-6.5	-2.5
14	5'-CG CAA CZC AAC GC	52.5 (-3.0)	-11.0	-6.5	-6.0
15	5'-CG CAA GZG AAC GC	52.5 (-2.5)	-8.0	-12.0	-8.0
16	5'-CG CAA TZT AAC GC	45.0 (-3.5)	-9.5	-10.0	-3.0

[a] T_m values measured as maximum of first derivative plot of melting curves (A_{260} vs. T) recorded in medium salt buffer solution ($[Na^+] = 110$ mM, $[Cl^-] = 100$ mM, pH 7.0 (NaH_2PO_4/Na_2HPO_4), EDTA = 0.2 mM) using 1.0 μ M concentration of each strand. T_m values are averages of at least two measurements. [b] (ΔT_m) = change in T_m value relative to unmodified reference duplex for example, **ON5:DNA** versus **ON1:DNA**. [c] Mismatch ΔT_m = difference in T_m value between mismatched duplex and complementary duplex; mismatched sequences: 3'-GC GTT TBT TTG CG-5' (for **ON1/ON5/ON9/ON13**), 3'-GC GTT GBG TTG CG-5' (for **ON2/ON6/ON10/ON14**), 3'-GC GTT CBC TTG CG-5' (for **ON3/ON7/ON11/ON15**) and 3'-GC GTT ABA TTG CG-5' (for **ON4/ON8/ON12/ON16**) where **B** is A, C, G, and T.

ditional insight into the binding mode of the fluorophore, we recorded absorption, steady-state fluorescence emission ($\lambda_{ex} = 344$ nm) and fluorescence excitation ($\lambda_{em} = 404$ nm) spectra of single stranded probes (SSPs) **ON5–ON16** and of the corresponding duplexes with complementary or mismatched DNA targets. Low experimental temperatures (5°C) were chosen to maximize strand hybridization. Deoxygenation was deliberately not applied to the samples since the scope of the work was to determine fluorescence enhancement under aerated conditions prevailing in bioassays. In addition, cross-calibrated fluorescence emission quantum yields (Φ_F) were determined relative to pyrenebutanoic acid in methanol ($\Phi_F = 0.065$)^[17] and 9,10-diphenylanthracene in cyclohexane ($\Phi_F = 0.95$)^[18] following established protocols (see the Supporting Information).^[17]

Hybridization of **ON5–ON16** to complementary DNA is accompanied by a) hypsochromic shifts in absorption and excitation maxima of the pyrene moiety of 3–7 nm from approximately 345–350 nm to approximately 342–346 nm (Figure 2, as well as Figures S4 and S5, and Table S3 and S4 in the Supporting Information), b) increases in extinction coefficients (hyperchromic shifts) that appear to be most pronounced for α -L-LNA monomer **Z** and least pronounced for DNA monomer **X** (Table 2), and c) formation of duplexes that exhibit broad fluorescence emission maxima at approximately 402 nm with a shoulder at approximately 387 nm (Figure 3 as well as Figures S6–S8 and Table S5 in the Supporting Information). Duplex formation between

ONs modified with DNA monomer **X** (**ON5–ON8**) and complementary DNA is accompanied with 2.4- to 9.6-fold increases in fluorescence intensity (see values above black histograms in Figure 4 upper panel) and high fluorescence quantum yields ($\Phi_F = 0.33$ –0.58, Table 2). In concert, these observations suggest decreased electronic interactions between pyrene and quenching nucleobase moieties upon duplex formation.^[19] ONs modified with LNA monomer **Y** (**ON9–ON12**) display similar hybridization-induced increases in fluorescence intensity (Figure 4 middle panel) but form duplexes with even higher quantum yields, particularly in the **CYC**- and **GYG**-sequence contexts (**ON10** and **ON11**, Table 2). Interestingly, ONs modified with α -L-LNA monomer **Z** display larger hybridization-induced increases in fluo-

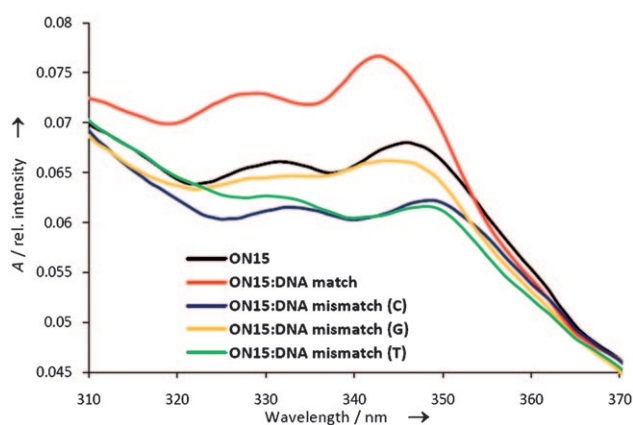


Figure 2. Absorption spectra of **ON15** and duplexes with matched or mismatched DNA targets (mismatched nucleotide opposite of incorporation site mentioned in parenthesis). Buffers and conditions are as described for T_m experiments, $T = 5^\circ\text{C}$.

rescence intensity in the **AZA**- and **TZT**-contexts than corresponding ONs modified with **X** or **Y** monomers (e.g., compare **ON8/ON12/ON16**, Figure 4 lower panel), while similar increases are observed in the other sequence contexts. In addition, duplexes display the highest observed quantum yields in this study ($\Phi_F = 0.50$ –0.80, Table 2) which suggests that the fluorophore experiences even fewer quenching interactions with nucleobases. This is most likely a consequence of a more rigid positioning of the fluoro-

Table 2. Fluorescence quantum yields (Φ_F) and extinction coefficients ϵ_{344} of **ON5–ON16** in the absence (SSP) or presence of matched or mismatched DNA targets.^[a]

ON	Sequences	SSP	Φ_F ($\epsilon_{344\text{nm}}$ [$\text{cm}^{-1} \text{mM}^{-1}$])			
			B=A	C	G	T
5	5'-CG CAA AXA AAC GC	0.21 (22)	0.44 (24)	0.31 (17)	0.10 (17)	0.16 (16)
6	5'-CG CAA CXC AAC GC	0.16 (19)	0.43 (24)	0.08 (17)	0.08 (16)	0.09 (18)
7	5'-CG CAA GXG AAC GC	0.04 (19)	0.33 (20)	0.04 (17)	0.05 (15)	0.03 (17)
8	5'-CG CAA TXT AAC GC	0.17 (21)	0.58 (23)	0.32 (18)	0.15 (17)	0.12 (16)
9	5'-CG CAA AYA AAC GC	0.32 (19)	0.48 (23)	0.47 (17)	0.16 (15)	0.45 (16)
10	5'-CG CAA CYC AAC GC	0.27 (20)	0.67 (29)	0.14 (18)	0.09 (16)	0.12 (17)
11	5'-CG CAA GYG AAC GC	0.04 (25)	0.44 (29)	0.02 (20)	0.07 (20)	0.04 (20)
12	5'-CG CAA TYT AAC GC	0.31 (20)	0.61 (28)	0.62 (17)	0.17 (18)	0.31 (16)
13	5'-CG CAA AZA AAC GC	0.17 (11)	0.53 (16)	0.22 (8)	0.25 (11)	0.07 (9)
14	5'-CG CAA CZC AAC GC	0.23 (20)	0.61 (30)	0.19 (17)	0.24 (23)	0.10 (14)
15	5'-CG CAA GZG AAC GC	0.08 (23)	0.50 (31)	0.05 (20)	0.27 (27)	0.05 (16)
16	5'-CG CAA TZT AAC GC	0.28 (12)	0.80 (20)	0.44 (9)	0.40 (14)	0.17 (9)

[a] Conditions as described in footnote of Table 1. $\lambda_{\text{ex}} = 344 \text{ nm}$, $T = 5^\circ\text{C}$, $1.0 \mu\text{M}$ concentration of each strand.

phore in the major groove. Similar observations have been reported for LNA analogues linked to fluorophores that point to the minor groove.^[10f,20]

Next, the optical properties of mismatched duplexes were studied. Pronounced bathochromic shifts of pyrene absorption (2–8 nm, Figure 2, and Table S3) and fluorescence emission maxima (up to 5 nm, Figure 3 as well as Figures S6–S8 and Table S5 in the Supporting Information) were observed relative to matched duplexes along with large hypochromic shifts in pyrene absorption (Table 2). This points toward increased interactions between pyrene and nucleobase moieties in mismatched duplexes,^[19] which is indicative of an increasingly intercalative binding mode of the pyrene fluorophore.^[8d,10b,21]

Probes where DNA monomer **X** is incorporated between flanking cytosine or guanine moieties (**ON6** & **ON7**) display excellent optical discrimination of SNPs (Figure 3 left panel and Figure S7) with large discrimination factors I_m/I_{mm} of 7.4–8.4 and 9.7–12.9 (values above blue/yellow/green histograms in Figure 4 upper panel, see legend for definition of I_m/I_{mm}). Less efficient discrimination is observed in **AXA**-

and **TXT**-sequence contexts, which demonstrates the need for nearby guanine moieties to quench pyrene monomer fluorescence^[15b,22] and ensure efficient SNP discrimination. ONs modified with LNA monomer **Y** generally display improved SNP discrimination in the **CYC**- and **GYG**-sequence contexts ($I_m/I_{\text{mm}} = 7.3$ – 15.9 and 8.3 – 41.9 for **ON10** and **ON11**, respectively, Figure 4 middle panel) but less efficient discrimination in the **AYA**- and **TYT**-sequence contexts. By contrast, ONs modified with α -LNA monomer **Z** (**ON13–ON16**) display distinctly different fluorescence trends than **ON5–ON12**, for example, the **Z**:G-mismatches are the least efficiently discriminated mismatches (Figure 4 lower panel). This behaviour is surprising given the aforementioned efficiency of guanine to quench pyrene monomer fluorescence^[15b,22] and that other SNP-typing probes discriminate G-mismatches well.^[8d,g,h] Moreover, improved SNP discrimination is observed in the challenging **AZA**- and **TZT**-contexts although higher discrimination factors, in particular with G-mismatches, would be desirable for practical diagnostic applications ($I_m/I_{\text{mm}} = 3.4$ – 14.1 and 2.9 – 11.4 for **ON13** and **ON16**, respectively, Figure 3 right panel and Figure 4 lower panel).

Interestingly, the observed intensity-based mismatch discrimination factors of **ON5–ON16** are not fully accounted by the differences in quantum yields between matched and mismatched duplexes, for example, compare $I_m/I_{\text{mm}} = 5.8$ with $\Phi_{F,m}/\Phi_{F,\text{mm}} = 0.61/0.19 \approx 3.2$ for **ON14** versus the C-mismatched target (Figure 4 and Table 2, respectively). This reflects the fact that fluorescence brightness depends on the emission quantum yield Φ_F and the extinction coefficient ϵ of the fluorophore, which is markedly lower in mismatched

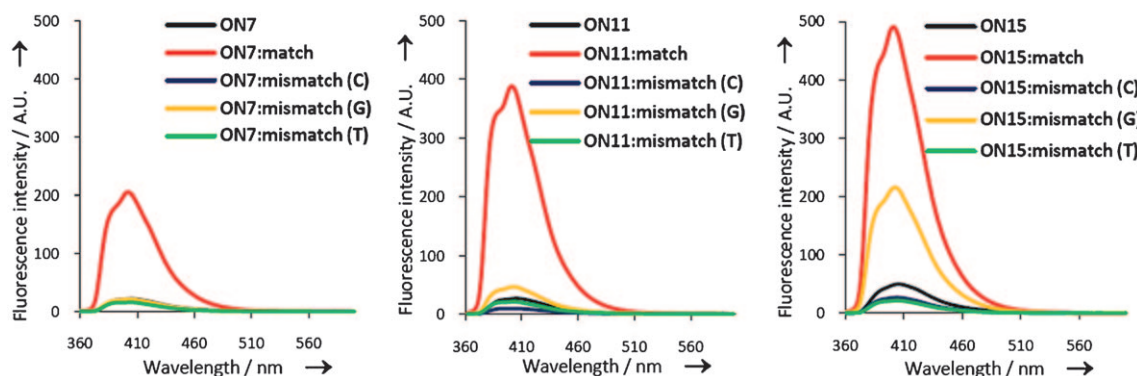


Figure 3. Steady-state fluorescence spectra of **ON7** (left), **ON11** (middle) and **ON15** (right) in the absence or presence of matched or mismatched DNA targets (mismatched nucleotide opposite of incorporation site mentioned in parenthesis). Buffers and conditions are as described for T_m experiments. $\lambda_{\text{ex}} = 344 \text{ nm}$; $T = 5^\circ\text{C}$, $1.0 \mu\text{M}$ concentration of each strand.

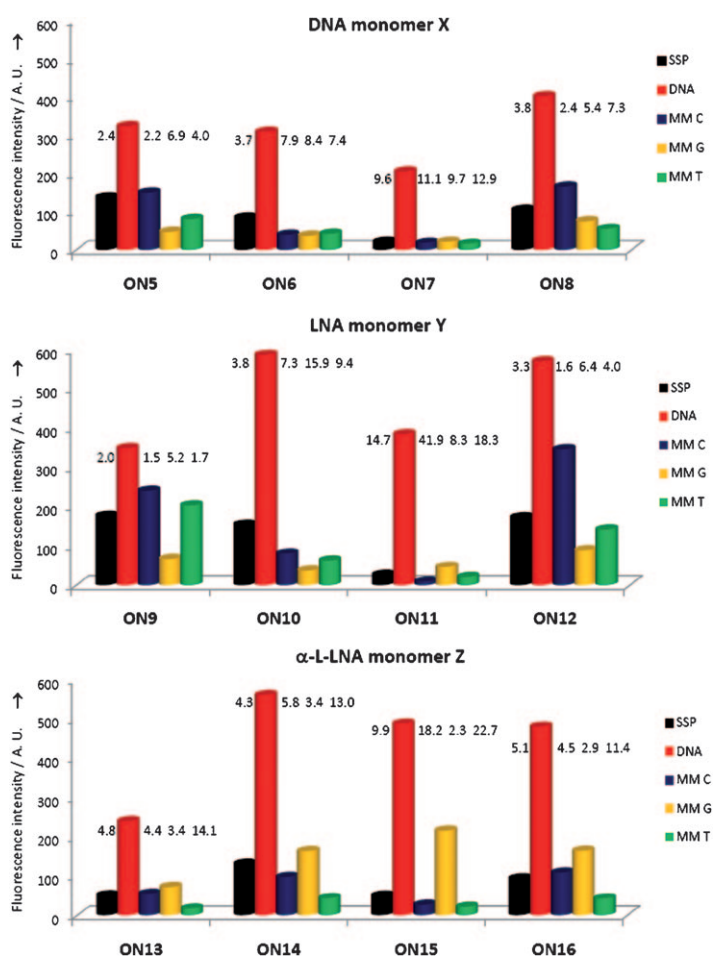


Figure 4. Fluorescence intensity of ON5–ON16 in the absence (SSPs) or presence of complementary DNA or mismatched DNA targets. Panels depict ONs modified with monomer X (upper), monomer Y (middle), or monomer Z (lower). Hybridization-induced increases and discrimination factors (I_m/I_{mm}), defined as the fluorescence intensity of duplexes with complementary DNA divided by the intensity of SSPs or duplexes with mismatched DNA, respectively, are listed above corresponding histograms. Intensity recorded at $\lambda_{em}=402$ nm at $T=5^\circ\text{C}$, $1.0\ \mu\text{M}$ concentration of each strand.

duplexes than in matched duplexes (Table 2). It is particularly noteworthy that larger relative differences in extinction coefficients between matched and mismatched duplexes are observed with ON9–ON16 (LNA and α -L-LNA monomers Y and Z) than with ON5–ON8. This demonstrates that a) decreased quantum yields in tandem with lower extinction coefficients of mismatched duplexes bring about the SNP discrimination of monomers X–Z, and b) conformational restriction of the furanose skeleton translates into altered emission output of polarity-sensitive fluorophores conjugated to the C5 position of pyrimidines.

Hybridization to RNA targets: Motivated by these results and the importance of fluorescent probes in the elucidation of biological functions of RNA,^[23] we set out to study the physical properties of duplexes between probes in the representative CBC- and TBT-sequence contexts and comple-

mentary or singly mismatched RNA targets. Similar trends in duplex thermostability (see Table S6), target specificity (see Table S6), excitation maxima (see Table S8), and hybridization-induced increases in fluorescence intensity (see Figures S11–S13) are observed as in the corresponding studies with DNA targets. However, the optical discrimination of mismatched RNA targets is generally much less efficient (see Figure S13) which is accompanied by higher quantum yields for mismatched duplexes (see Table S7). These observations point toward less facile intercalation of the pyrene moiety in mismatched RNA duplexes, possibly due to the more compressed DNA:RNA duplex architectures^[24] which leads to less efficient nucleobase-mediated quenching. Probes modified with monomer X or Y display similar optical discrimination of RNA-mismatches, whereas monomer Z modified probes display slightly improved discrimination in the TZT-context (see Figure S13, lower panel). Matched duplexes involving ONs modified with LNA monomer Y or α -L-LNA monomer Z exhibit higher quantum yields than with monomer X (see Table S7).

Integrated discussion: The results demonstrate that probes based on LNA monomer Y offer practical advantages as SNP-detection probes compared to the original 5-[3-(1-pyrene-carboxamido)propynyl]-2'-deoxyuridine probes (monomer X) in CYC- and GYG-sequence contexts (higher quantum yields and improved optical discrimination of SNPs). Probes modified with α -L-LNA monomer Z, on the other hand, display interesting characteristics in the challenging AZA- and TZT-contexts (larger hybridization-induced increases, higher quantum yields and improved optical discrimination of SNPs). Results from optical spectroscopy studies strongly suggest that the nucleobase moieties of monomers X–Z adopt *anti* and *syn* conformations upon hybridization with matched and mismatched targets, respectively. The polarity-sensitive 1-pyrene-carboxamido fluorophore is thereby either positioned in the polar major groove or in the hydrophobic duplex core close to quenching nucleobases. The improved SNP-discrimination by LNA and α -L-LNA monomers Y and Z, is a consequence of higher emission quantum yields of matched duplexes (monomers Y and Z), high pyrene extinction coefficients in matched duplexes (monomer Y), and low pyrene extinction coefficients in mismatched duplexes (monomer Z). Calculations indicate that the bicyclic skeletons of the LNA and α -L-LNA monomers Y and Z influence the glycosidic torsional angle profile through steric hindrance between H6 and sugar hydrogens and, thereby, the positioning and photophysical properties of the C5-fluorophore (see Figure S14 in the Supporting Information).

Conclusion

The study provides important insight into the fluorescence properties of SNP-typing probes utilizing 5-[3-(1-pyrene-carboxamido)propynyl]pyrimidines as base discriminating fluorescent monomers. First, efficient optical discrimination of

SNPs by ONs modified with known BDF monomer **X** is demonstrated to necessitate nearby guanine moieties. Second, conformational restriction of the furanose skeleton (monomers **Y** and **Z**) translates into altered emission output of polarity-sensitive fluorophores appended to the C5 position of pyrimidines, which reflects changes in quantum yields and extinction coefficients of the fluorophore. Accordingly, probes modified with LNA and α -L-LNA monomers **Y** and **Z** display more beneficial SNP-typing characteristics. We envision that the use of ONs modified with LNA/ α -L-LNA monomers conjugated to polarity-sensitive fluorophores via short rigid linkers is a promising strategy toward development of probes for sequence-unrestricted SNP-typing.

Experimental Section

General: All reagents and solvents were of analytical grade and obtained from commercial suppliers and used without further purification. Petroleum ether of the distillation range 60–80 °C was used. Anhydrous dichloromethane, 1,2-dichloroethane, and *N,N*-diisopropylethylamine (DIPEA) were dried through storage over activated 4 Å molecular sieves. Water content of the anhydrous solvents was checked by a Karl-Fischer apparatus. Reactions were conducted under an atmosphere of argon whenever anhydrous solvents were used. All reactions were monitored by thin-layer chromatography (TLC) using silica gel coated plates with fluorescence indicator (SiO₂-60, F-254) which were visualized a) under UV light or, b) by dipping in 5% conc. sulfuric acid in absolute ethanol (v/v) followed by heating. Silica gel column chromatography was performed with silica gel 60 (particle size 0.040–0.063 mm) using moderate pressure (pressure ball). Silica gel columns were built with an initial starting eluent containing 1% (v/v) of pyridine. Evaporation of solvents was carried out under reduced pressure at temperatures below 50 °C. After column chromatography, appropriate fractions were pooled, evaporated and dried at high vacuum for at least 12 h to give the obtained products in high purity (>95%) which was ascertained by 1D NMR techniques. Chemical shifts of ¹H NMR (500 MHz), ¹³C NMR (125 MHz), and ³¹P NMR (121.5 MHz) spectra are reported in parts per million (ppm) relative to deuterated solvent or other internal standards (80% phosphoric acid for ³¹P NMR, respectively). Exchangeable (ex) protons were detected by disappearance of peaks on D₂O addition. Assignments of NMR spectra are based on 2D spectra (COSY, HSQC) and DEPT spectra. Quaternary carbons were not assigned but verified from HSQC and DEPT spectra (absence of signals). The carbon atom of C4' substituents is numbered C5''. Similar conventions apply for the corresponding hydrogen atoms. Assignments of ¹H NMR signals of H5' and H5'' and the corresponding ¹³C NMR signals are interchangeable. ESI-HRMS spectra of compounds dissolved in a saturated solution of NaCl in CH₃CN with PEG as an internal calibrant, were recorded on a Quadrupole Time-Of-Flight tandem Mass Spectrometer (Q-TOF Premiere).

(1R,3R,4R,7S)-1-(4,4'-Dimethoxytrityloxymethyl)-7-hydroxy-3-[5-[3-(1-pyrenecarboxamido)propynyl]uracil-1-yl]-2,5-dioxabicyclo[2.2.1]heptane (2Y): Nucleoside **1Y** (0.50 g, 0.73 mmol), [Pd(PPh₃)₄] (90 mg, 0.07 mmol), CuI (30 mg, 0.14 mmol), and *N*-(prop-2-ynyl)pyrene-1-carboxamide^[8d] (0.28 g, 1.00 mmol) were added to anhydrous DMF (10 mL) and the resulting mixture was degassed and placed under argon. To this was added Et₃N (0.40 mL, 2.84 mmol) and the reaction mixture was stirred at room temperature for 12 h whereupon solvents were evaporated off. The resulting residue was taken up in EtOAc (100 mL) and sequentially washed with brine (2 × 50 mL) and sat. aq. NaHCO₃ (50 mL). The combined aqueous phase was back-extracted with EtOAc (100 mL), and the combined organic phase was dried (Na₂SO₄), evaporated to dryness and the resulting crude residue purified by column chromatography (0–5% MeOH in CH₂Cl₂ (v/v)) to afford the nucleoside **2Y** (0.45 g,

74%) as a light yellow solid. *R*_f = 0.5 (5% MeOH in CH₂Cl₂, v/v); ESI-HRMS: *m/z*: 862.2778 ([*M*+Na]⁺, C₅₁H₄₁N₃O₉+Na, calcd 862.2735); ¹H NMR ([D₆]DMSO): δ = 1.71 (s, 1H, ex, NH), 9.95 (t, 1H, ex, *J* = 5.5 Hz, NHCH₂), 8.52–8.54 (d, 1H, *J* = 9.5 Hz, Ar), 8.21–8.36 (m, 6H, Ar), 8.09–8.13 (m, 2H, Ar), 7.84 (s, 1H, H₆), 7.23–7.46 (m, 9H, Ar), 6.90 (d, 4H, *J* = 9.0 Hz, Ar), 5.73 (d, 1H, ex, *J* = 4.5 Hz, 3'-OH), 5.45 (s, 1H, H1'), 4.20–4.34 (m, 3H, H2', CH₂NH), 4.07 (d, 1H, *J* = 4.5 Hz, H3'), 3.82–3.83 (d, 1H, *J* = 8.0 Hz, H5''), 3.80–3.81 (d, 1H, *J* = 8.0 Hz, H5'), 3.72 (s, 6H, 2 × OCH₃), 3.57–3.59 (d, 1H, *J* = 11.0 Hz, H5'), 3.29–3.31 ppm (d, 1H, *J* = 11.0 Hz, H5'); ¹³C NMR ([D₆]DMSO): δ = 168.5, 161.8, 158.12, 158.07, 149.0, 144.7, 141.6 (C6), 135.5, 134.9, 131.7, 131.0, 130.7, 130.1, 129.9 (Ar), 129.6 (Ar), 128.3 (Ar), 128.1 (Ar), 127.90 (Ar), 127.89, 127.5 (Ar), 127.1 (Ar), 126.7 (Ar), 126.5 (Ar), 125.8 (Ar), 125.2 (Ar), 124.6 (Ar), 124.3 (Ar), 123.7, 123.6, 113.3 (Ar), 113.2 (Ar), 97.8, 89.4, 87.6, 87.0 (C1'), 85.6, 78.8 (C2'), 74.6, 71.4 (C5'), 69.7 (C3'), 59.1 (C5''), 54.98 (OCH₃), 54.97 (OCH₃), 29.5 ppm (CH₂NH).

(1S,3R,4S,7R)-1-(4,4'-Dimethoxytrityloxymethyl)-7-hydroxy-3-[5-[3-(1-pyrenecarboxamido)propynyl]uracil-1-yl]-2,5-dioxabicyclo[2.2.1]heptane (2Z): Nucleoside **1Z** (0.50 g, 0.73 mmol), [Pd(PPh₃)₄] (90 mg, 0.07 mmol), CuI (30 mg, 0.14 mmol), *N*-(prop-2-ynyl)pyrene-1-carboxamide^[8d] (0.28 g, 1.00 mmol), and Et₃N (0.40 mL, 2.84 mmol) in anhydrous DMF (10 mL) were allowed to react, worked up, and purified as described for **2Y** to provide nucleoside **2Z** (0.47 g, 79%) as a light yellow solid material. *R*_f = 0.5 (5% MeOH in CH₂Cl₂, v/v); ESI-HRMS: *m/z*: 862.2756 ([*M*+Na]⁺, C₅₂H₄₁N₃O₉ Na⁺, calcd 862.2735); ¹H NMR ([D₆]DMSO): δ = 11.77 (s, 1H, ex, NH), 9.23 (t, 1H, ex, *J* = 5.5 Hz, NHCH₂), 8.54–8.55 (d, 1H, *J* = 9.5 Hz, Ar), 8.19–8.35 (m, 6H, Ar), 8.10–8.14 (m, 2H, Ar), 7.99 (s, 1H, H₆), 7.13–7.40 (m, 9H, Ar), 6.88 (d, 4H, *J* = 9.0 Hz, Ar), 5.98 (s, 1H, H1'), 5.95 (d, 1H, ex, *J* = 4.5 Hz, 3'-OH), 4.49 (d, 2H, *J* = 5.5 Hz, CH₂NH), 4.43 (d, 1H, *J* = 4.5 Hz, H3'), 4.28 (s, 1H, H2'), 4.03–4.05 (d, 1H, *J* = 8.5 Hz, H5''), 3.95–3.97 (d, 1H, *J* = 8.5 Hz, H5'), 3.69 (s, 6H, 2 × CH₃O), 3.32 ppm (s, 2H, H5'); ¹³C NMR ([D₆]DMSO): δ = 168.6, 161.7, 158.1, 149.3, 144.7, 143.0 (C6), 135.2, 135.1, 131.7, 131.0, 130.7, 130.1, 129.79 (Ar), 129.67 (Ar), 128.3 (Ar), 128.1 (Ar), 127.9 (Ar), 127.8 (Ar), 127.5 (Ar), 127.1 (Ar), 126.6 (Ar), 126.5 (Ar), 125.8 (Ar), 125.6 (Ar), 125.2 (Ar), 124.5 (Ar), 124.3 (Ar), 123.8, 123.6, 113.2 (Ar), 97.1, 89.5, 89.4, 87.1 (C1'), 85.3, 78.7 (C2'), 74.5, 72.8 (C3'), 72.4 (C5''), 59.8 (C5'), 54.9 (CH₃O), 29.6 ppm (CH₂NH).

(1R,3R,4R,7S)-1-(4,4'-Dimethoxytrityloxymethyl)-3-[5-[3-(1-pyrenecarboxamido)propynyl]uracil-1-yl]-2,5-dioxabicyclo[2.2.1]heptane (3Y): Alcohol **2Y** (0.25 g, 0.29 mmol) was coevaporated with anhydrous 1,2-dichloroethane (2 × 10 mL) and dissolved in anhydrous CH₂Cl₂. To this was added DIPEA (0.19 mL, 1.50 mmol), and 2-cyanoethyl-diisopropylchlorophosphoramidite (PCI reagent) (0.09 mL, 0.38 mmol) and the reaction mixture was stirred at room temperature for 2 h. The reaction mixture was diluted with CH₂Cl₂ (25 mL), washed with 5% aq. NaHCO₃ (2 × 10 mL), and the combined aqueous phase back-extracted with CH₂Cl₂ (2 × 10 mL). The combined organic phase was dried (Na₂SO₄), evaporated to dryness, and the resulting crude residue purified by column chromatography (0–2% MeOH/CH₂Cl₂, v/v) to provide phosphoramidite **3Y** (190 mg, 61%) as a white foam. *R*_f = 0.5 (2% MeOH in CH₂Cl₂, v/v); ESI-HRMS: *m/z*: 1062.3807 ([*M*+Na]⁺, C₆₀H₅₈N₅O₁₀P-Na⁺, calcd 1062.3814); ³¹P NMR (CDCl₃, 121.5 MHz): δ = 149.7, 149.2 ppm.

(1S,3R,4S,7R)-1-(4,4'-Dimethoxytrityloxymethyl)-3-[5-[3-(1-pyrenecarboxamido)propynyl]uracil-1-yl]-2,5-dioxabicyclo[2.2.1]heptane (3Z): Nucleoside **2Z** (0.44 g, 0.52 mmol), DIPEA (0.46 mL, 2.6 mmol), and 2-cyanoethyl-diisopropylchlorophosphoramidite (0.18 mL, 0.78 mmol) in anhydrous CH₂Cl₂ (10 mL) were allowed to react, worked up, and purified as described for **3Y** to furnish phosphoramidite **3Z** (0.41 g, 75%) as a white foam. *R*_f = 0.5 (2% MeOH in CH₂Cl₂, v/v); ESI-HRMS: *m/z*: 1062.3790 ([*M*+Na]⁺, C₆₀H₅₈N₅O₁₀P-Na⁺, calcd 1062.3814); ³¹P NMR (CDCl₃, 121.5 MHz): δ = 150.3, 149.8 ppm.

Oligonucleotide synthesis: Oligonucleotides (ONs) were synthesized on a 0.2 μmol scale using an Expedite 8909 Synthesizer and succinyl-linked LCAA-CPG (long-chain alkyl amine controlled pore glass) columns with a pore size of 500 Å. Standard procedures were used, that is, trichloro-

acetic acid in CH_2Cl_2 as detritylation reagent; 0.25 M 4,5-dicyanoimidazole (DCI) in anhydrous CH_3CN as activator; acetic anhydride in THF as cap A solution; 1-methylimidazole in THF/pyridine (8:1, v/v) as cap B solution, and 0.02 M iodine in H_2O /pyridine/THF as the oxidizing solution. Incorporation of monomers **X–Z** into ONs was accomplished by extended coupling (15 min) of the corresponding phosphoramidites **3X–Z** with DCI as the activator, which resulted in coupling yields above 98%. Cleavage from the solid support and removal of protecting groups was accomplished by treatment with concentrated aqueous ammonia (55 °C, 24 h). Purification of all modified ONs was performed to minimum 80% purity using either of two methods: a) overall synthesis yield > 80%: cleavage of DMT using 80% aq. AcOH, followed by precipitation from acetone (–18 °C for 12–16 h) and washing with acetone, or b) overall synthesis < 80%: purification of ONs by RP-HPLC using a gradient of 0.05 M triethyl ammonium acetate in water and 25% water in acetonitrile (see Table S1 in the Supporting Information), followed by detritylation and precipitation as outlined above.

Purification of crude ONs was performed on a Varian Prostar HPLC system equipped with an XTerra MS C18 column (10 μm , 7.8 \times 150 mm) using the representative gradient protocol depicted in Table S1. The composition of all synthesized ONs was verified by MALDI MS analysis (see Table S2) recorded in positive ion mode on a Quadrupole Time-Of-Flight tandem Mass Spectrometer (Q-TOF Premiere) equipped with a MALDI source (Waters Micromass LTD., U.K.) using 2,5-dihydroxybenzoic acid as a matrix and PEG as an internal standard. Purity (> 80%) was verified by RP-HPLC.

Protocol for thermal denaturation studies: Concentrations of unmodified ONs were estimated using the following extinctions coefficients for DNA (OD/ μmol): G (12.01), A (15.20), T (8.40), C (7.05); for RNA (OD/ μmol): G (13.70), A (15.40), U (10.00), C (9.00). Concentrations of modified ONs (**ON5–ON16**) were determined by titration with complementary DNA; a progressive increase in steady-state fluorescence emission intensity was observed until a plateau was reached, at which point a 1:1 stoichiometry was assumed. This approach was crossvalidated by comparison with conventional methods for concentration determination of pyrene-functionalized ONs which assume an ϵ_{260} of 22.4 OD/ μmol for the pyrene moiety.^[10b] The two methods gave concentration determinations within ($\pm 10\%$). ONs (1.0 nmol of each strand, 1 μM) were thoroughly mixed, denatured by heating and subsequently cooled to the starting temperature of the experiment. Quartz optical cells with a pathlength of 1.0 cm were used. Thermal denaturation temperatures (T_m values [°C]) were measured on a Cary 100 UV/VIS spectrophotometer equipped with 12-cell Peltier temperature controller and determined as the maximum of the first derivative of the thermal denaturation curve (A_{260} vs. T) recorded in medium salt buffer (T_m buffer: 110 mM NaCl, 0.1 mM EDTA, pH adjusted with 10 mM $\text{Na}_2\text{HPO}_4/\text{NaH}_2\text{PO}_4$). The temperature of the denaturation experiments ranged from at least 15 °C below T_m to 20 °C above T_m (although not below 1 °C). A temperature ramp of 0.5 °C min^{–1} was used in all experiments. Reported thermal denaturation temperatures are an average of at least two experiments within (± 1.0) °C.

Protocol for fluorescence studies: Steady state fluorescence emission spectra were recorded using a Cary Eclipse fluorimeter using the same buffers and ON concentrations (1.0 μM) as in thermal denaturation studies. Fluorescence emission spectra of single stranded probes (SSP) and corresponding duplexes with complementary or mismatched targets were measured at 5 °C to ensure maximal hybridization. Deoxygenation was deliberately not applied to the samples since the scope of the work was to determine fluorescence under aerated condition prevailing in biosays. Solutions were heated to 80 °C over 10 min, cooled to 5 °C over 15 min, and equilibrated at this temperature for more than 5 min. Steady-state fluorescence emission spectra (360–600 nm range) were obtained as an average of five scans using an excitation wavelength of 344 nm, excitation slit 5.0 nm, emission slit 5.0 nm and a scan speed of 600 nm min^{–1}. The fluorescence quantum yield Φ_F of pyrenebutanoic acid (PBA) in MeOH in this experimental setting was measured to be 0.069 relative to 9,10-diphenylanthracene in cyclohexene ($\Phi_F = 0.95$),^[17] which is in excellent agreement with the reported value of 0.065.^[18] Emission quantum yields Φ_F (ON) of single-stranded **ON9–ON12** and the corresponding du-

plexes with DNA/RNA targets were determined according to Equation (1),

$$\Phi_F(\text{ON}) = \Phi_F(\text{PBA}) \times [A(\text{ON})/A_{344}(\text{ON})] \times [1/\alpha(\text{PBA})] \times [n(\text{H}_2\text{O})^2/n(\text{MeOH})^2]^{17} \quad (1)$$

where $\Phi_F(\text{PBA})$ is the cross-calibrated value for the fluorescence quantum yield of PBA in MeOH, $A(\text{ON})$ is the area of the fluorescence emission spectrum of the sample from 360 to 600 nm, $A_{344}(\text{ON})$ is the absorbance of the sample at the excitation wavelength (344 nm), $\alpha(\text{PBA})$ is the slope of the fluorescence emission versus $A_{344}(\text{ON})$ calibration curve for PBA and $n(\text{H}_2\text{O})$ and $n(\text{MeOH})$ are the refractive indexes of water (1.3328) and methanol (1.3288), respectively. The reported quantum yields are an average of at least two measurements within ($\pm 10\%$), although low quantum yields ($\Phi_F < 10\%$) may be associated with considerably larger error.

Fluorescence excitation spectra were recorded using the same buffer and concentrations as for the thermal denaturation studies at $T = 5$ °C. 402 nm was used as the emission wavelength and excitation intensity was scanned from 300 to 400 nm.

Acknowledgements

We appreciate financial support from Idaho NSF EPSCoR, the BANTech Center at the University of Idaho, and a scholarship from the College of Graduate Students, University of Idaho (M.E.Ø.). We thank the EBI Murdock Mass Spectrometry Center for mass spectrometric analyses. F.M.Y. thanks IBEST and BANTech at the University of Idaho for computing resources.

- [1] S. Kim, A. Misra, *Annu. Rev. Biomed. Eng.* **2007**, *9*, 289–320.
- [2] C. Ahlborn, K. Siegmund, C. Richert, *J. Am. Chem. Soc.* **2007**, *129*, 15218–15232.
- [3] a) N. Venkatesan, Y. J. Seo, B. H. Kim, *Chem. Soc. Rev.* **2008**, *37*, 648–663; b) K. Wang, Z. Tang, C. J. Yang, Y. Kim, X. Fang, W. Li, Y. Wu, C. D. Medley, Z. Cao, J. Li, P. Colon, H. Lin, W. Tan, *Angew. Chem.* **2009**, *121*, 870–885; *Angew. Chem. Int. Ed.* **2009**, *48*, 856–870.
- [4] a) D. M. Kolpashchikov, *Chem. Rev.* **2010**, *110*, 4709–4723; b) P. L. Paris, J. M. Langenhan, E. T. Kool, *Nucleic Acids Res.* **1998**, *26*, 3789–3793; c) A. A. Marti, S. Jockusch, N. Stevens, J. Ju, N. J. Turro, *Acc. Chem. Res.* **2007**, *40*, 402–409; d) T. Umamoto, P. J. Hrdlicka, B. R. Babu, J. Wengel, *ChemBioChem* **2007**, *8*, 2240–2248.
- [5] a) A. P. Silverman, E. T. Kool, *Chem. Rev.* **2006**, *106*, 3775–3789; b) T. N. Grossmann, O. Seitz, *Chem. Eur. J.* **2009**, *15*, 6723–6730.
- [6] a) U. B. Christensen, E. B. Pedersen, *Helv. Chim. Acta* **2003**, *86*, 2090–2097; b) O. Köhler, D. Venkatrao, D. V. Jarikote, O. Seitz, *ChemBioChem* **2005**, *6*, 69–77; c) T. S. Kumar, J. Wengel, P. J. Hrdlicka, *ChemBioChem* **2007**, *8*, 1122–1125.
- [7] a) A. A. Gorodetsky, M. C. Buzzeo, J. K. Barton, *Bioconjugate Chem.* **2008**, *19*, 2285–2296; b) L. Valis, N. Amann, H. A. Wagenknecht, *Org. Biomol. Chem.* **2005**, *3*, 36–38; c) E. Mayer-Enthart, H. A. Wagenknecht, *Angew. Chem.* **2006**, *118*, 3451–3453; *Angew. Chem. Int. Ed.* **2006**, *45*, 3372–3375; d) C. Wanninger-Weiss, L. Valis, H. A. Wagenknecht, *Bioorg. Med. Chem.* **2008**, *16*, 100–106.
- [8] a) A. Okamoto, Y. Saito, I. Saito, *J. Photochem. Photobiol. C* **2005**, *6*, 108–122; b) D. W. Dodd, R. H. E. Hudson, *Mini-Rev. Org. Chem.* **2009**, *6*, 378–391; c) K. Yamana, H. Zako, K. Asazuma, R. Iwase, H. Nakano, A. Murakami, *Angew. Chem.* **2001**, *113*, 1138–1140; *Angew. Chem. Int. Ed.* **2001**, *40*, 1104–1106; d) A. Okamoto, K. Kanatani, I. Saito, *J. Am. Chem. Soc.* **2004**, *126*, 4820–4827; e) G. T. Hwang, Y. J. Seo, S. J. Kim, B. H. Kim, *Tetrahedron Lett.* **2004**, *45*, 3543–3546; f) R. H. E. Hudson, A. Ghorbani-Choghamarani, *Org. Biomol. Chem.* **2007**, *5*, 1845–1848; g) M. E. Østergaard, D. C. Guenther, P. Kumar, B. Baral, A. J. Paszczyński, P. K. Sharma, P. J. Hrdlicka, *Chem. Commun.* **2010**, *46*, 4929–4931; h) S. S. Bag, R.

- Kundu, K. Matsumoto, Y. Saito, I. Saito, *Bioorg. Med. Chem. Lett.* **2010**, *20*, 3227–3230; i) Y. Shinohara, K. Matsumoto, K. Kugenuma, T. Morii, Y. Saito, I. Saito, *Bioorg. Med. Chem. Lett.* **2010**, *20*, 2817–2820.
- [9] A. Okamoto, K. Tainaka, Y. Ochi, K. Kanatani, I. Saito, *Mol. Bio-Syst.* **2006**, *2*, 122–126.
- [10] a) T. S. Kumar, A. S. Madsen, M. E. Østergaard, J. Wengel, P. J. Hrdlicka, *J. Org. Chem.* **2008**, *73*, 7060–7066; b) T. S. Kumar, A. S. Madsen, M. E. Østergaard, S. P. Sau, J. Wengel, P. J. Hrdlicka, *J. Org. Chem.* **2009**, *74*, 1070–1081; c) M. E. Østergaard, P. Kumar, B. Baral, D. J. Raible, T. S. Kumar, B. A. Anderson, D. C. Guenther, L. Deobald, A. J. Paszczynski, P. K. Sharma, P. J. Hrdlicka, *ChemBioChem* **2009**, *10*, 2740–2743; d) S. P. Sau, P. Kumar, B. A. Anderson, M. E. Østergaard, L. Deobald, A. Paszczynski, P. K. Sharma, P. J. Hrdlicka, *Chem. Commun.* **2009**, 6756–6758; e) S. P. Sau, T. S. Kumar, P. J. Hrdlicka, *Org. Biomol. Chem.* **2010**, *8*, 2028–2036; f) M. E. Østergaard, P. Cheguru, M. R. Papasani, R. A. Hill, P. J. Hrdlicka, *J. Am. Chem. Soc.* **2010**, *132*, 14221–14228.
- [11] a) A. A. Koshkin, S. K. Singh, P. Nielsen, V. K. Rajwanshi, R. Kumar, M. Meldgaard, C. E. Olsen, J. Wengel, *Tetrahedron* **1998**, *54*, 3607–3630; b) S. Obika, T. Uneda, T. Sugimoto, D. Nanbu, T. Minami, T. Doi, T. Imanishi, *Bioorg. Med. Chem.* **2001**, *9*, 1001–1011; c) H. Kaur, B. R. Babu, S. Maiti, *Chem. Rev.* **2007**, *107*, 4672–4697.
- [12] M. D. Sørensen, L. Kværnø, T. Bryld, A. E. Håkansson, B. Verbeure, G. Gaubert, P. Herdewijn, J. Wengel, *J. Am. Chem. Soc.* **2002**, *124*, 2164–2176.
- [13] a) M. Petersen, C. B. Nielsen, K. E. Nielsen, G. A. Jensen, K. Bondensgaard, S. K. Singh, V. K. Rajwanshi, A. A. Koshkin, B. M. Dahl, J. Wengel, J. P. Jacobsen, *J. Mol. Recognit.* **2000**, *13*, 44–53; b) M. Petersen, A. E. Håkansson, J. Wengel, J. P. Jacobsen, *J. Am. Chem. Soc.* **2001**, *123*, 7431–7432.
- [14] W. Saenger, *Principles of Nucleic Acid Structure*, Springer, Berlin, **1984**.
- [15] a) V. A. Korshun, D. A. Stetsenko, M. J. Gait, *J. Chem. Soc. Perkin Trans. 1* **2002**, 1092–1104; b) C. Dohno, I. Saito, *ChemBioChem* **2005**, *6*, 1075–1081.
- [16] Y. You, B. G. Moreira, M. A. Behlke, R. Owczarzy, *Nucleic Acids Res.* **2006**, *34*, e60.
- [17] J. V. Morris, M. A. Mahaney, J. R. Huber, *J. Phys. Chem.* **1976**, *80*, 969–974.
- [18] T. L. Netzel, K. Nafisi, J. Headrick, B. E. Eaton, *J. Phys. Chem.* **1995**, *99*, 17948–17955.
- [19] G. Dougherty, J. R. Pilbrow, *Int. J. Biochem.* **1984**, *16*, 1179–1192.
- [20] a) P. J. Hrdlicka, B. R. Babu, M. D. Sørensen, N. Harrit, J. Wengel, *J. Am. Chem. Soc.* **2005**, *127*, 13293–13299; b) D. Honcharenko, C. Zhou, J. Chattopadhyaya, *J. Org. Chem.* **2008**, *73*, 2829–2842; c) I. V. Astakhova, V. A. Korshun, J. Wengel, *Chem. Eur. J.* **2008**, *14*, 11010–11026.
- [21] M. Nakamura, Y. Fukunaga, K. Sasa, Y. Ohtoshi, K. Kanaori, H. Hayashi, H. Nakano, K. Yamana, *Nucleic Acids Res.* **2005**, *33*, 5887–5895.
- [22] M. Manoharan, K. L. Tivel, M. Zhao, K. Nafisi, T. L. Netzel, *J. Phys. Chem.* **1995**, *99*, 17461–17472.
- [23] S. Tyagi, *Nat. Methods* **2009**, *6*, 331–338.
- [24] V. Marin, H. F. Hansen, T. Koch, B. A. Armitage, *J. Biomol. Struct. Dyn.* **2004**, *21*, 841–850.

Received: July 23, 2010

Revised: November 16, 2010

Published online: February 15, 2011